A >200 ka U-Th based chronology from lacustrine evaporites, Searles Lake, CA

Justin S. Stroup[1,2], Kristian J. Olson[3], Tim K. Lowenstein[3], Adam B. Jost[2], Hayley M. Mosher[1], Mark D. Peaple[4], Sarah J. Feakins[4], Christine Y. Chen[5], Steven P. Lund[4], David McGee[2]

[1]Department of Atmospheric and Geological Sciences, State University of New York at Oswego, Oswego, NY 13126

[2]Department of Earth, Atmospheric and Planetary Sciences, Massachusetts Institute of Technology, Cambridge, MA 02139

[3]Department of Geological Sciences and Environmental Studies, State University of New York, Binghamton, New York 13902, USA

[4]Department of Earth Sciences, University of Southern California, Los Angeles, CA 90089

[5]Chemical and Isotopic Signatures Group, Division of Nuclear and Chemical Sciences, Lawrence Livermore National Laboratory, Livermore, CA, USA

Highlights:

- **>200 ka-long sediment record of southwestern North American paleoenvironment**
- **Establishes criteria for selection of evaporite minerals for U-Th dating**
- **Explores a wide range of parameters for Bayesian age-depth modeling**

Abstract

Well-dated lacustrine records are essential to establish the timing and drivers of regional hydroclimate change. Searles Basin, California records the depositional history of a fluctuating saline-alkaline lake in the terminal basin of the Owens River system draining the eastern Sierra Nevada. Here we establish a U-Th chronology for the ~76-m-long SLAPP-SLRS17 core collected in 2017 based on dating of evaporite minerals. 98 dated samples comprising 9 different minerals were evaluated based on stratigraphic, mineralogic, textural, chemical and reproducibility criteria. After application of these criteria, a total of 37 dated samples remained as constraints for the age model. A lack of dateable minerals between 145–110 ka left the age model unconstrained over the penultimate glacial termination (Termination II). We thus established a tie point between plant wax δD values in the core and a nearby speleothem $\delta^{18}O$ record at the beginning of the Last Interglacial. We construct a Bayesian age model allowing stratigraphy to inform sedimentation rate inflections. We find the >210 ka SLAPP-SRLS17 record contains five major units that correspond with prior work. The new dating is broadly consistent with previous efforts but provides more precise age estimates and a detailed evaluation of evaporite depositional history. We also offer a substantial revision of the age of the Bottom Mud-Mixed Layer contact, shifting it from ~130 ka to 178±3 ka. The new U-Th chronology documents the timing of mud and salt layers and lays the foundation for climate reconstructions.

Keywords: U-Th series, Geochronology, Age Model, Evaporite Minerals, Searles Lake, Owens River

Plain language summary

Searles Lake, CA is currently a dry saltpan; however, in the past, it was a large and deep lake (>200 m). Lake levels have varied with changes in climate. These changes influenced the sediments deposited. Thus, changes in the lake sediments can be applied to understand the past environments of the region. Here, we developed a chronology for a 76 m-long core using isotopic dating methods. The lake sediments contain many different minerals which can be age dated. However, some of these minerals formed after the lake sediments were deposited, and others have been chemically altered in the time since their formation. We developed criteria for selection of samples that are the most likely to reflect the age of sediment deposition. We used the selected ages along with statistical modeling to determine the ages of the sediments with depth. We find the core contains a record that spans over 200,000 years, including the last two glacial cycles. The age model presented here lays the foundation for exploration of how past climate changes impacted water availability and vegetation in southeastern California.

1 Introduction

Southwestern North America experienced pronounced changes in precipitation and water availability during Late Pleistocene glacial-interglacial cycles. A diverse array of paleoclimate archives, including lake deposits, speleothems, and packrat middens, document how lake levels, water tables, vegetation, and precipitation patterns have varied (e.g., Bader, 2000; Heusser et al., 2015; Lachniet et al., 2014; Litwin et al., 1999; Lowenstein et al., 1999; Moseley et al., 2016; Oster et al., 2014; Reheis et al., 2014; Thompson and Anderson, 2000; Wendt et al., 2018; Woolfenden, 2003). These archives provide benchmarks that can be used to test how well

climate models represent the response of regional hydroclimate to a range of forcings and boundary conditions (e.g., Lora et al., 2017; McGee et al., 2018; Oster et al., 2015; Tabor et al., 2021).

The sedimentary record of the Searles Basin (southeastern California) is a particularly important target for further development (Figure 1). The basin has been the terminus of the Owens River system for much of the last several hundred thousand years (Smith, 1979). Since the Owens River is a leading source of water for the Los Angeles metropolitan area, data from Searles Basin are important for documenting how the water balance of a societally important watershed has responded to past climate changes.

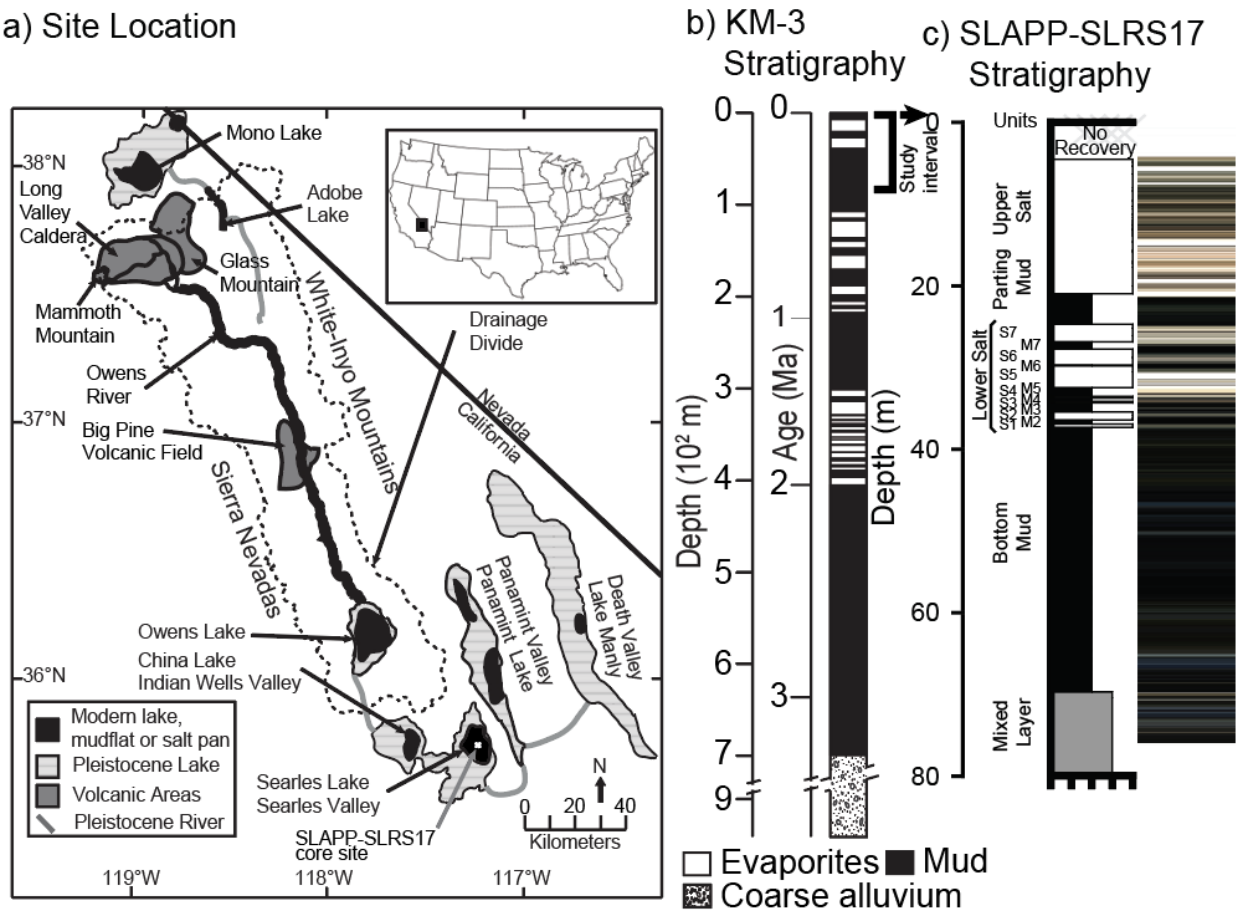

Figure 1. a) The Searles Basin is located in the Owens River drainage in the southern Sierra Nevada mountain range (California, USA). It is the third basin in a chain of five basins that spilled into one another at times in the past. b) The KM-3 core stratigraphy demonstrates that the Searles Basin contains a long sediment record, ~700 m spanning the last ~3.3 Ma. The general stratigraphy has been extensively documented (e.g., Liddicoat et al., 1980; Smith, 1979). c) SLAPP-SLRS17 stratigraphic column (units established from prior work) and core color composite which highlights many small-scale stratigraphic changes not represented in the general stratigraphy. Light colors are evaporite-dominated sediments and darker colors indicate muds; note in many cases the mud contains abundant evaporite minerals.

Previous work demonstrated that Searles Basin deposits record dramatic changes in water balance. Lake shoreline deposits range up to ~200 m above the presently dry basin floor, and sediments from the last glacial period preserve millennial-scale oscillations between salt and mud (Lin et al., 1998; Peng et al., 1978; Phillips et al., 1994; Smith, 1979, 2009). In addition, the basin contains a long sediment record, reaching back to the late Pliocene (3.3 Ma) (Liddicoat et al., 1980). Studies of the more recent Late Pleistocene sediments lay the foundation for explorations of the region's more ancient paleoclimate.

Previous work also presents a conundrum that motivates further development of the Late Pleistocene record from the Searles Basin. During the last glacial period, lake levels in basins across the southwestern U.S., including the Searles and Owens basins, appear to have been high, prior to drying after ~15 ka during the last deglaciation (Bacon et al., 2006; Bacon et al., 2020; Benson et al., 1990; Munroe and Laabs, 2013; Reheis et al., 2014; Rosenthal et al., 2017). Data from nearby Death Valley suggest a similar pattern during previous glacial periods, with higher lake and water table levels during the penultimate glacial period and drying during Termination II (~130 ka) (Ku et al., 1998; Lowenstein et al., 1999; Wendt et al., 2018). In contrast, Searles

Basin sediments have been interpreted to indicate lake deepening rather than drying during Termination II, with deep lakes during the last interglacial period (Bischoff et al., 1985; Smith, 1984). While this inconsistency has been noted for over 30 years, it remains undetermined whether it results from chronological problems, errors in sedimentological interpretation, or actual climatic or hydrological differences.

Establishing chronologies in evaporite lacustrine environments can be particularly challenging because of sedimentological, mineralogical, and technical considerations. In these environments, sediments are especially susceptible to diagenetic interactions which must be understood to interpret the timing of sediment deposition and to select syndepositional material for dating. Prior chronologic work (Bischoff et al., 1985; Lin et al., 1998; Peng et al., 1978; Phillips et al., 1994; Phillips et al., 1983; Smith, 2009) assumed that the materials dated were syndepositional. In many cases, they were also technologically limited by U-Th methods (alpha decay counting in earlier studies, and analysis by thermal ionization mass spectrometry in later studies) which required larger sample sizes (0.5 g to >10 g) that integrated different minerals. Thus, samples were dated without detailed petrographic study. Researchers recognized spurious ages (e.g., Smith, 2009) and identified inconsistencies in existing chronologies (e.g., Knott et al., 2019). While each study advanced the understanding of the region and provided additional layers of chronological information, none established a robust framework for interpreting syndepositional minerals for dating. Olson and Lowenstein (2021) explore the complexities of sedimentation and diagenesis within the Searles Basin. This work, along with technological advancements that allow dating of small samples, highlights a need to reassess prior work and provides a pathway for the present study.

This study seeks to enable deeper exploration of the Searles Basin sediment record through the development of an age model for two sediment cores collected near the center of the basin in 2017. We combine U-Th dating of lake precipitates with interpretations of the depositional and diagenetic history of dated samples to obtain robust depositional ages. Using Bayesian age modeling, we apply these ages and one tie point based on a comparison of SLAPP-SRLS17 plant wax hydrogen isotope (δD_{wax}) data and the "Leviathan" speleothem $\delta^{18}O$ record (Lachniet, 2016) to establish an age-depth relationship that serves as the foundation for proxy records from the core. We anticipate that this work will renew investigation of the basin's response during the penultimate glacial period, Termination II, and the last interglacial, as well as the application of proxies that were not available during previous coring of the basin (e.g., organic biomarkers;Peaple et al., 2022)

2 Stratigraphy and Previous Dating

The subsurface stratigraphy of Searles Lake is characterized by interbedded muds and salts which record hydrologic variability. Muds were deposited during relatively wet periods and salts formed during dry periods (net evaporation > net inflow). The Lower Salt is subdivided into 7 salt layers and 6 mud layers, and the Mixed Layer is subdivided into 9 units, A-I.

Previous work used radiocarbon and U-Th dating to provide age estimates for the uppermost ~250 ka of Searles Basin sedimentation. All radiocarbon ages from previous work have been recalibrated using INTCAL20 (Reimer et al., 2020), and all U-Th ages have been recalculated using updated decay constants (Cheng et al., 2013) and an initial atomic $^{230}Th/^{232}Th$ ratio of $9\pm4 \times 10^{-6}$ (see below for explanation of this initial value).

Dates from the surface through the Upper Salt span from 3.8±0.3 ka (^{14}C date on a wood fragment; Smith (1979) to 8.8±2.5 ka (U-Th date on salt; Peng et al., 1978), placing this unit within the Holocene. Radiocarbon dating using decay counting of disseminated organic matter in the Parting Mud indicated a basal age of 27 ka and a top age of 12.3 ka (Smith, 1979), roughly corresponding to the Last Glacial Maximum and deglaciation. We treat these as estimates due to the potential for modern carbon contamination during extraction of bulk organic matter to bias ages younger, and the potential for lake reservoir effects and inputs of pre-aged organic carbon to bias ages older.

Previous U-Th dating of the Lower Salt unit indicated that this interval spans ~35 to 23 ka (Lin et al., 1998; Peng et al., 1978; Phillips et al., 1994). Though the dates have substantial uncertainties and there are some disagreements between U-Th datasets (Supplementary Figure S1), the existing U-Th data from the Upper Salt suggest that the basal age of the Parting Mud is ~23 ka, not 27 ka. Phillips et al. (1994) and Lin et al. (1998) suggested that the seven salt units in the Upper Salt correspond to millennial-scale warming events recorded in Greenland ice cores (Interstadials 2-8). Lin et al. (1998) carefully evaluated the initial ^{230}Th/^{232}Th ratio for Searles Basin salts, finding that a value of 9×10^{-6} (corresponding to an activity ratio of 1.8) is required to preserve stratigraphic order in U-Th ages from the Lower Salt unit.

Bischoff et al. (1985) used U-Th dating of gaylussite, dolomite and trona to extend the age model through the Bottom Mud and uppermost Mixed Layer. Their data placed the Bottom Mud-Mixed Layer contact at around 130 ka, near the time of Termination II, and suggested that the Mixed Layer extends beyond 250 ka. Smith (2009) reexamined these ages along with the ^{36}Cl-based age estimates of Jannik et al. (1991), and suggested that the basal age for the Bottom Mud was closer to ~150 ka.

Together, existing data from the Searles Basin suggest much lower sedimentation rates of muds than salts. Sedimentation rates in the Upper Salt approach 1 m/ka, whereas rates in the Parting Mud and Bottom Mud are approximately 0.2-0.3 m/ka. However, substantial uncertainties remain in the age-depth relationship due to low precision of individual ages, substantial scatter in Bottom Mud and upper Mixed Layer ages, and a lack of detailed characterization of the minerals being dated.

3 Evaporite minerals in the Searles Basin

Development of a Searles Lake age model requires an understanding of the timing and mechanisms of mineral formation. The chemical sediments of core SLAPP-SRLS17 are composed of 14 major minerals (carbonates, sulfates, borates, silicates, and chlorides) each of which exhibits a variety of depositional and post-depositional textures (Table 1; Figure S2-S7). Identifying textures indicative of post-depositional alteration is crucial to using saline minerals for geochronologic analysis.

Mineral	Formula	Environment				Timing			Texture			Sedimentological Assessment of U/Th Ages
		Water Column	Lake Floor	Subsurface		Primary	Syndepositional	Burial	Non-porous	Porous		
				Shallow	Deep					Permeable	Impermeable	
Halite	NaCl		X			X			X			Reliable
Aragonite	$CaCO_3$	X				X					X	
Gaylussite	$Na_2Ca(CO_3)_2 \cdot 5H_2O$			X			X		X			
Pirssonite	$Na_2Ca(CO_3)_2 \cdot 2H_2O$			X			X		X			
Trona	$Na_3H(CO_3)_2 \cdot 2H_2O$	X				X	?	?		X		Unreliable
Nahcolite	$NaHCO_3$	X				X	?	?		X		
Burkeite	$Na_6(CO_3)(SO_4)_2$	X				X	?	?	X			
Borax	$Na_2(B_4O_5)(OH)_4 \cdot 8H_2O$	X		?	X	X	?	?	X			
Hanksite	$Na_{22}K(SO_4)_9(CO_3)_2Cl$			?	X		?	?	X			
Aphthitalite	$(K,Na)_3Na(SO_4)_2$	X				X			X			Not Dated
Calcite	$CaCO_3$	X				X					X	
Dolomite	$CaMg(CO_3)_2$	X		X		X	X				X	
Northupite	$Na_3Mg(CO_3)_2Cl$			X			X		X			
Thenardite	Na_2SO_4		X			X	X	?	X			

Table 1. List of common minerals in the SLAPP-SLRS17 sediments and characterization of qualities relevant to interpretations of U-Th ages.

Olson and Lowenstein (2021) used Pitzer-based thermodynamic models to reproduce the mineral phases, sequences, and abundances observed in core SLAPP-SRLS17 as a function of (1) evaporative concentration of Owens River inflow water, (2) temperature, (3) salinity, (4) pCO_2, and (5) thermodynamic system behavior (*open* or *closed*). Core and thin section textures and fabrics were used to distinguish between primary (cumulate and bottom-growth) and secondary (replacement, cement) minerals. The geochemical and sedimentological analyses were then integrated for each mineral to interpret the environment of deposition (water column, lake floor, shallow subsurface, or deep subsurface), timing of formation (primary, syndepositional, or burial), and chemical processs involved (direct crystallization or back-reaction).

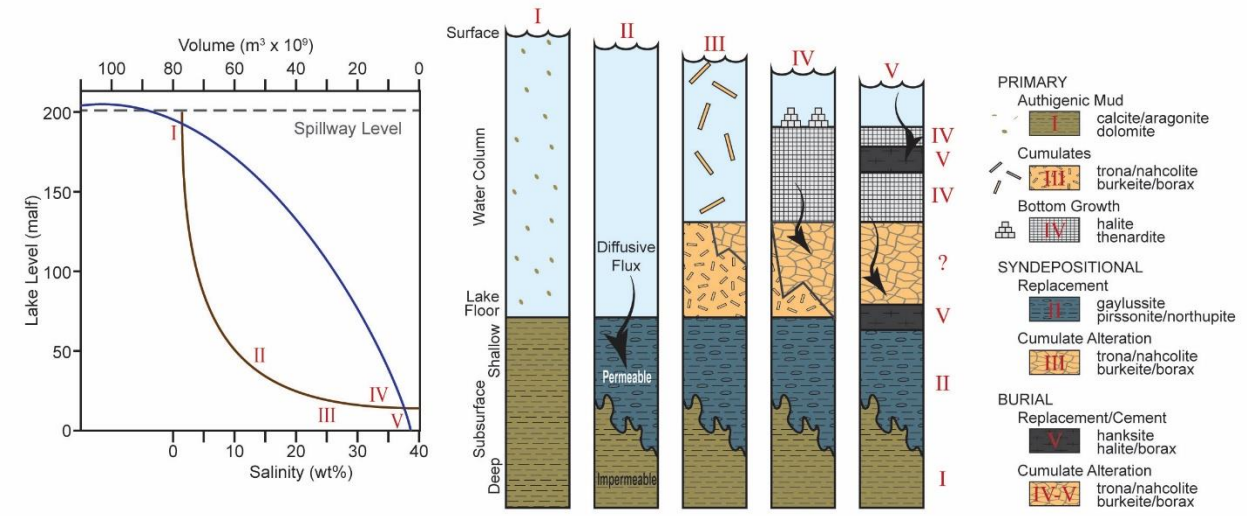

Figure 2. Schematic of mineral formation histories. (Left) Lake volume and salinity relationships with corresponding facies (I–V). (Right) Facies and depositional history diagram. I) Large lake conditions result in lower salinities and authigenic mud deposition; II) smaller lake conditions cause increased salinities, creating a density gradient between lake water and pore fluid that drives displacive crystal growth in existing sediments;

III, IV and V) further reductions in lake volume increase salinity initiating evaporite precipitation and further cementation. Arrows indicate density-driven infiltration of pore fluids by more saline lake bottom water.

The general Searles Lake depositional model is as follows. First, alkaline earth carbonates calcite/aragonite [$CaCO_3$] and dolomite [$CaMg(CO_3)_2$] precipitate in the water column and are deposited on the lake floor as massive or laminated chemical muds (Figure 2-I; S3). As lake level falls and salinity increases, saline-alkaline brines sink along density gradients into the underlying lake sediment. The resulting increase in porewater salinity drives in-situ, *closed* system back-reactions, with gaylussite [$Na_2Ca(CO_3)_2 \cdot 5H_2O$] replacing calcite/aragonite and northupite [$Na_3Mg(CO_3)_2Cl$] replacing dolomite (Figure 2-II; S3). Downward diffusion of high salinity brines drives reaction with gaylussite to produce pirssonite [$Na_2Ca(CO_3)_2 \cdot 2H_2O$]. Brine diffusion is limited by sediment compaction such that gaylussite, northupite, and pirssonite likely form syndepositionally, near the sediment/water interface (Olson and Lowenstein, 2021).

As evaporation continues, Searles Lake brine reaches salt saturation and trona, nahcolite, burkeite, and borax precipitate within the water column and settle onto the lake floor as cumulates (Figure 2-III; S4). As Searles Lake brines reach their maximum concentration, halite [NaCl] and thenardite [$NaSO_4$] precipitate directly on the lake floor as bottom-growth (Figure 2-IV; S6). Void-filling cements are the last to form (Figure 2-V). Hanksite [$Na_{22}K(SO_4)_9(CO_3)_2Cl$] is the predominant void-filling cement and can form by multiple back-reactions depending on the available precursor salts (Olson and Lowenstein, 2021). Hanksite is found at cumulate/mud boundaries and near dense halite layers, suggesting hanksite forms where dense, downward moving brines encounter impermeable layers (Figure S7). Large volumes of hanksite cement suggest pre-compaction formation, but the precise timing is unclear.

The depositional model above focuses on how and when each mineral formed from evolving Searles Lake surface brine. Post-depositional processes also influenced salt preservation in the subsurface of Searles Lake. Cumulates which precipitate seasonally may back-react on the lake floor to equilibrate at bottom water temperatures (Figure 2-III). Cumulate alteration may also occur during early diagenesis due to changes in pore-water chemistry (Figure 2-IV), or during late diagenesis as deposits equilibrate to burial temperatures (Figure 2-V). Thus, while the models of Olson and Lowenstein (2021) establish a framework for interpreting the formation of each mineral, additional work is required to characterize post-depositional processes before the radiometric age of each mineral is interpreted. Here, additional sedimentological analysis is applied to core SLAPP-SRLS17 to identify textures indicative of diagenesis and establish criteria for evaluating the reliability o f Searles Lake minerals for U-Th geochronology.

4 Methods

4.1 Core collection and description

The Searles Lake Paleoclimate Project (SLAPP) collected two cores using sonic drilling in 2017. The first, SLAPP-SRLS17-1A (35.73715 ˚N, -117.33029 ˚W), extended to 76.7 m below the surface (mbs), and the second (SLAPP-SRLS17-2A, 35.73715 ˚N, -117.33033˚W) extended from 21.7 mbs to 38.8 mbs to provide continuous coverage of millennial-scale salt-mud oscillations in the Lower Salt. Core description, sampling, scanning and photography were completed at the Continental Scientific Drilling (CSD) Facility (formerly the National Lacustrine Core Facility) at the University of Minnesota, Twin Cities, in 2017 (Figure 1C). Gray scale data

was extracted from core images using ImageJ. The images were collected directly after core splitting to minimize oxidation. All images were collected with a constant exposure. The data were also used to assemble core color composites. These data are intended to represent the more detailed stratigraphy of the core record not captured by the major stratigraphic units. The SLAPP-SRLS17 cores preserve stratigraphy recognized from previous work in the basin (Smith, 1979, 2009; Smith et al., 1983), from bottom to top including the uppermost Mixed Layer, Bottom Mud, Lower Salt, Parting Mud and Upper Salt units (Figure 1). The stratigraphy of SLAPP-SRLS17 closely corresponds to the core KM-3, ~10 m away (Smith et al., 1983).

4.2 Sample selection and preparation

Of the 14 major/minor SLAPP minerals, 5 were excluded from dating (Table 1). Calcite and dolomite were excluded due to sample impurities (low U/Th ratios) as well as uncertainties regarding detrital vs authigenic and primary vs diagenetic origins. Northupite crystals could not be cleanly separated from muddy matrix due to their small, sub-millimeter size. Aphthitalite [$(K,Na)_3Na(SO_4)_2$] is typically found encased in hanksite cement, from which it could not be cleanly separated. Bottom-growth thenardite was found in a single layer, but initial screening (section 4.3) revealed U/Th atomic ratios of ~1, too low for U/Th analysis. Dating attempts were made on the remaining 9 minerals (Table 1).

Once a dating horizon and mineral were identified, crystals were handpicked and precleaned to remove detrital material. The evaporite crystals were covered in sediment (mud, other mineral grains) which was removed by rinsing, sonicating, and mixing by vortex repeatedly in pure ethanol to clean the exterior of the crystals. The samples were scrubbed and

rinsed with a small paint brush and ethanol squirt bottle until the exteriors of the crystals were clean of loose debris.

We then evaluated the crystals under a binocular microscope. Crystals with many sediment inclusions were rejected. The exteriors of sediment-free crystals or solid crystal masses were scraped and/or cleaved to separate the interior for dating. This helped eliminate debris that was stuck on crystal surfaces and minimize exterior surfaces that may have recrystallized (that would produce younger ages) or lost uranium (that would cause ages to be older). Each crystal was then cleaved into smaller portions and inspected for additional inclusions, signs of secondary crystallization (smaller infilling crystals), or fluid penetration (cracks). Clean crystal fragments were collected until enough material was gathered for U-Th screening and dating.

Sample materials were identified by XRD and visual inspection. Sample mineralogies are indicated in the data archived at the NOAA paleoclimatology database. XRD was done on most samples used for dating. We did not perform XRD on the exact material dated for samples 44, 51, 71, and 73 (listed as halite & borax) and samples 24, 45, 48, 49, and 74 (listed as halite & trona); for these samples, XRD was done on the bulk material prior to cleaning and picking samples. These samples, however, are thought to be pure halite; if they contained trace amounts of trona or borax, they would still be considered minimum depositional ages.

4.3 U-Th analysis

We screened most samples for their ^{238}U and ^{232}Th concentrations to identify samples with relatively low detrital contamination and to estimate the amount of material and spike required for high-precision U-Th analyses. For screening, we isolated ~1 mg subsamples and dissolved them in 1.5 mL of 0.5 M nitric acid. If undissolved solids were observed after one hour of

reaction time, we used a pipette to remove ~1 mL of the solution and left behind the solids. We then introduced samples into a quadrupole ICP-MS (Agilent 7900) at MIT and measured ^{43}Ca, ^{232}Th, and ^{238}U. A standard containing Ca, U, and Th was analyzed at varying concentrations to establish a linear calibration between signal intensity and concentration, and the standard was analyzed after every ~15-20 samples to track calibration changes during the analytical session. Samples with atomic ^{238}U/^{232}Th ratios >10 were prioritized for U-Th dating, but we also dated samples with lower U/Th ratios in high-priority intervals. This screening allowed us to focus analyses on samples with low detrital contamination.

In addition, screening was important for determining sample weights necessary to achieve appropriate U contents (~10-100 ng) for U-Th dating, as U concentrations ranged from ~5 ng/g to 346 µg/g in our samples—almost 5 orders of magnitude. Due to this large range of concentrations, samples for dating ranged in mass from 0.2 to 593 mg (the average sample mass was 10 mg, and the median was 25 mg). We note that the small sample sizes used in this study represent an important advance over previous U-Th dating of Searles Basin deposits, as they allowed us to target particularly clean and/or dense material. Sample sizes in previous studies ranged from 0.5 g for TIMS-based analyses (Lin et al., 1998) to 10 g or more for decay-counting methods (Bischoff et al., 1985; Peng et al., 1978).

Samples selected for U-Th dating were processed using standard procedures in a clean laboratory at MIT (Supplementary Material). Measured U and Th isotope ratios were corrected for background, tailing, mass bias, ion counter yield, contributions of naturally occurring isotopes in the tracer, and procedural blank. Ages were determined using the ^{238}U half-life of Jaffey et al. (1971) and the ^{234}U and ^{230}Th half-lives of Cheng et al. (2013). Ages were corrected for contributions from initial ^{230}Th using the ^{230}Th/^{232}Th ratio determined by Lin et al. (1998)

317 from analyses of the Lower Salt (9 x 10^{-6} atomic). We assigned a 95% confidence interval of 4 x
318 10^{-6} to account for temporal variations in this ratio.

319 4.4 Age model development

320 We used the Bayesian modeling package Bacon (Blaauw and Christen, 2011; Trachsel and
321 Telford, 2017) for age-depth model construction because the multiple mud-salt transitions in the
322 Searles cores necessitated a model that can incorporate changing model parameters with
323 stratigraphic position. We used Bacon Version 2.5.7, which can accommodate extreme changes
324 in sedimentation rates and multiple stratigraphic units. Since model priors can be challenging to
325 set (Trachsel and Telford, 2017), we took an iterative approach to determine the various
326 parameters applied to generate age models. We ran more than 40 different combinations of
327 model configurations (Supplementary Material) to assess model parameter selection and the
328 impacts of our selection criteria. We compared model results against the U-Th age data,
329 stratigraphy and other model runs. We varied the initial parameters until the resulting age model
330 was no longer consistent with data or diverged. We compared the age model against the U-Th
331 ages and rejected parameter sets that caused the model to bypass viable ages, exhibit bias and/or
332 react too stiffly to unit changes. In cases of divergence, we found that some combinations of
333 parameters caused the mode to completely depart from the data. Based on these tests, we chose
334 the parameters that yielded solutions consistent with age and stratigraphic data, and we evaluated
335 a series of additional cross-parameter interactions and sensitivities.
336 The final model was constructed using the boundaries of each stratigraphic unit (Upper
337 Salt, Parting Mud, Lower Salt, Bottom Mud, Mixed Layer). It was particularly important to
338 select model sections (segments) that (1) matched unit thicknesses in the core; (2) used a small

value for memory to accommodate large changes in sedimentation regimes between evaporite and mud deposition; and (3) included appropriate initial accumulation rates for each unit. Age modeling parameters are described in the Supplementary Material. Several dating samples were from the same or nearby stratigraphic locations but were not from the same material. Thus, we treat them as individual ages in the Bacon model inputs. All ages are plotted individually in Figure 3.

5 Results:

5.1 Evaporite textures

Gaylussite and pirssonite occur as microscopic to cm-scale crystals in mud units. Crystals commonly contain non-calcareous inclusions. In laminated units, gaylussite crystals grow along and/or cross-cut laminations (Figure S3); a variety of growth fabrics occur in thin-bedded and massive units. Crystal textures varied among units but were typically uniform within a single depositional unit. However, in some instances, multiple populations of crystals were identified in a single unit by differing crystal morphology, orientation, or size.

Cumulates are defined as fine, well sorted, euhedral crystals which precipitate at the surface (rafts) or within the water column and then settle onto the lake floor. Layers with trona, nahcolite, halite, thenardite, aphthitalite, and borax meet these criteria. Cumulate layers are deposited with high primary porosity and are thus highly permeable except where cemented (See Supplementary Material Figures S3-S7 for more textural and mineralogical information). Trona and nahcolite display a variety of additional textures, including blades, splays, and overgrowths. Burkeite displays variable features but lacks unambiguous cumulate textures. Generally, burkeite

occurs as large vuggy masses composed of microcrystalline mosaics with abundant inclusions, typically trona cumulates. Burkeite can also be found as crystalline mosaics of interstitial material, some of which may be cement.

The textural criteria for recognizing halite bottom-growth are well established (Hardie et al., 1985; Lowenstein and Hardie, 1985). Bottom growth halite forms mm-scale crystals free of mud inclusions, typically associated with finely crystalline trona cumulates (Figure S6). In some cases, alteration of interstitial material results in dissolution and rounding of halite grain boundaries (Figure S5).

Pore-filling cements include hanksite, borax, and halite. Cements are typically free of mud inclusions. Hanksite and borax are also found in mud units. In these instances, borax occurs as large single crystals free of inclusions. In contrast, large hanksite crystals in mud units contain abundant included salts – typically cumulates of trona, thenardite, aphthitalite, borax, and halite.

5.2 U-Th ages

We determined a total of 98 U-Th ages on samples from SLAPP-SLRS17 cores (Data archived at the NOAA paleoclimatology database; Figure 3A). These ages include 23 replicates (samples of the same mineralogy and core depth). Samples included halite, gaylussite, nahcolite, trona, and aragonite, and ages ranged from 3.9 to 280 ka. The dataset suggests a general age-depth relationship that is broadly consistent with previous findings (e.g., Bischoff et al., 1985) (Supplementary Material), but several ages were not in stratigraphic order. To determine which U-Th results to include in the age model, we developed criteria to prioritize syndepositional minerals over post- or diagenetic minerals and identify ages least likely to have experienced open-system behavior with respect to U.

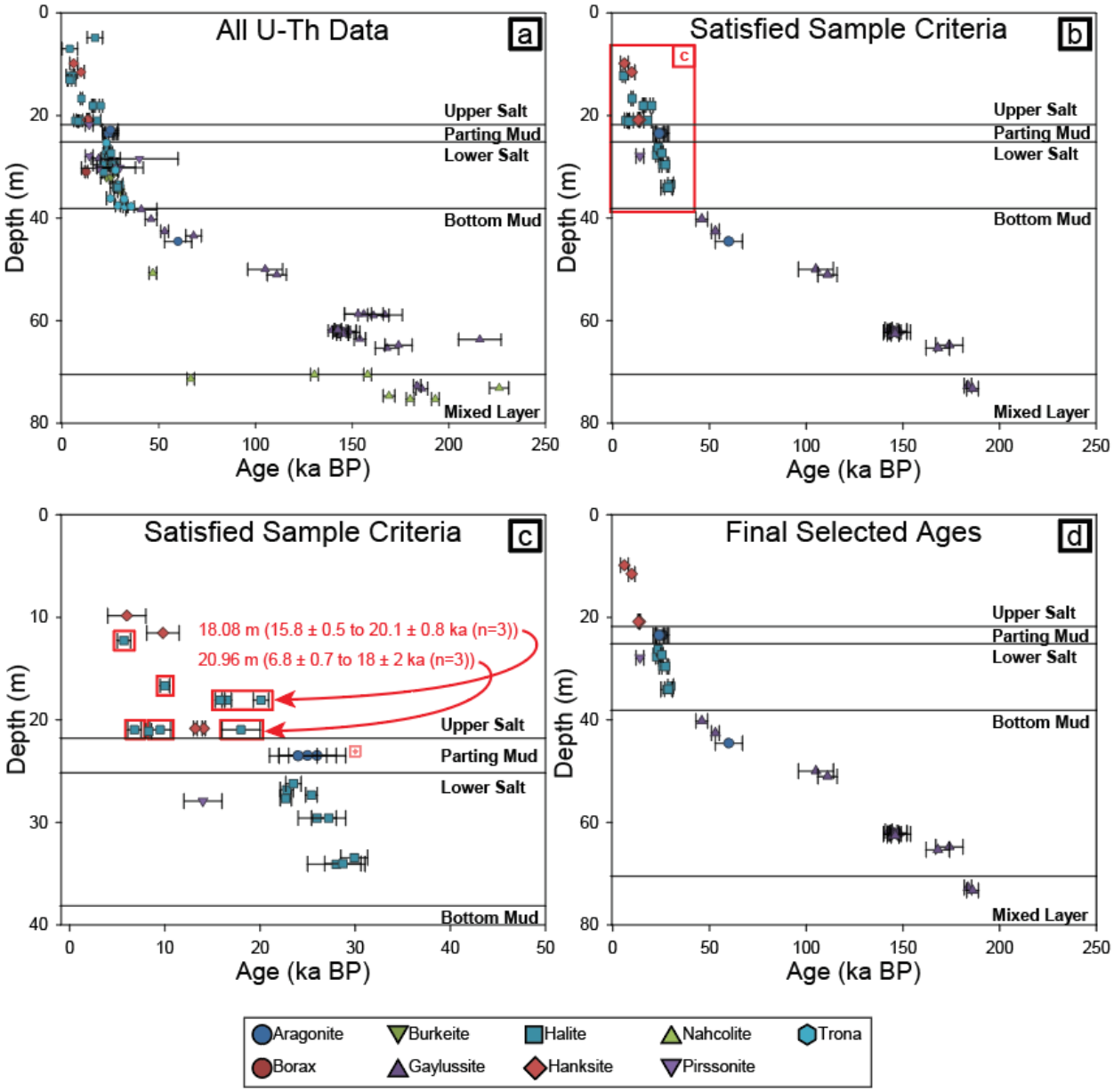

Figure 3. U-Th dating results. a) All U-Th results. Ninety-eight (98) samples from 11 mineral categories were dated. b) Forty-six ages that passed the sedimentological and U-Th criteria. Retained ages in the Mixed Layer, Bottom Mud and Lower Salt are internally consistent and reproducible. Halite ages in the Upper Salt (red box in c) show inconsistencies. c) Upper Salt ages, showing rejected halite

ages and hanksite ages retained as minimum depositional ages (see main text). d) Thirty-seven ages used for age modeling.

6 Discussion

6.1 Age evaluation

We developed and applied sedimentological and U-Th criteria to identify appropriate samples for chronology. We also considered the influences of past mining operations on the sediments to determine a selection of ages appropriate for age modeling.

6.1.1 Sedimentological criteria for age selection

The sedimentological criteria for age selection are based on the timing of mineral formation and suitability of minerals for U-Th geochemistry (Table 1). Additional sedimentological analysis is applied here to identify textures indicative of 1) post-depositional alteration and 2) possible *open* system behavior (i.e., uranium loss), both of which may impart age biases. Primary textures and low porosity are important considerations when selecting samples for U-Th dating because porous sediments with high hydraulic conductivity may allow leaching of soluble uranium from crystal boundaries, resulting in artificially older ages (Prado-Pérez et al., 2013). In the paragraphs that follow, we describe features (macroscopic and in thin section) that were used to determine which samples to include in the final age-depth model.

Early replacement minerals include gaylussite/pirssonite, which form via sediment/pore fluid back-reactions. Density-driven downward brine movement is predicted to occur during

periods when Searles Lake level fell and salinity increased. Such downward infiltration leads to replacement of calcite/aragonite by gaylussite, and later gaylussite replacement by pirssonite (Olson and Lowenstein, 2021). However, the dominant Ca-bearing mineral in Searles Lake is gaylussite; pirssonite is less common and calcite and aragonite occur in places (Figure S2-S3). This implies that downward diffusion of saline-alkaline brines and chemical interaction with muddy sediment did not proceed to completion. Olson and Lowenstein (2021) argue that early compaction of mud lowers permeability and limits downward brine flux. If so, gaylussite and pirssonite form syndepositionally, near the sediment-water interface, and should be appropriate for U-Th dating. Nonetheless, later diagenetic processes may produce gaylussite and pirssonite which requires additional examination to determine subsequent diagenetic varieties.

Gaylussite crystal size, abundance, and growth fabric are controlled by the amount and distribution of aragonite and calcite in mud layers. Gaylussite textures are therefore expected to vary from layer to layer, but should be uniform within indivdual layers. On the other hand, layers with multiple populations of gaylussite indicate several episodes of diagenetic crystal growth (Figure S3). Such units are excluded from age modeling. Although late diagenetic gaylussite is predicted to yield a younger age than the surrounding sediment, the opposite is true (Figure 5A, D). This suggests that subsurface brines interacted with and removed soluble uranium from gaylussite crystals, which produced older than true ages.

Most cumulate layers from the SLAPP-SLRS17 cores display textures indicative of diagenetic alteration (dissolution, overgrowth, replacement, recrystallization; Supplementary Material Section 3). Alteration of cumulates may occur syndepositionally due to seasonal brine temperature variations (Figure 2-III) or later as salts equilibrate with burial temperatures (Figure 2-V). Alteration may be enhanced by subsurface brine movement. In contrast to fine-grained

muds with low permeability, flow of brines through cumulate layers may be substantial because layers composed of randomly oriented crystals have exceedingly high porosity (Figure S4). Detailed sedimentological analysis of cumulates is therefore required to determine what criteria can be used to identify the timing and mechanisms of diagenetic alteration.

Many of the Searles Lake cumulates have been altered by dissolution, overgrowth, recrystallization, or replacement. The complex textures (Figure S4, S5) make it difficult to discern the timing of diagenesis. Cumulates with alteration textures are therefore excluded from age model consideration. In addition, the high porosity of all cumulates make such layers susceptible to open system uranium loss (Figure S4). Cumulates are therefore excluded from age model considerations, with the notable exception of aragonite laminae which occur in relatively impermeable units.

Primary bottom growth halite contains mud-free, mm-size single crystals. Bottom growth halite is therefore a good target for U–Th dating, although low U concentrations can make precise dating difficult (Table S1). Bottom growth halite is typically co-deposited with cumulates (Figure S6). In some cases, alteration of associated cumulate crystals produced dissolution and rounding of halite grain boundaries (Figure S5). Crystal boundaries are easily avoided during sampling (see section 5.5).

Cements composed of hanksite are mud free and therefore ideal for U-Th dating. However, it is not possible to distinguish the precise timing of cement formation (Hardie et al., 1983). Hanksite cements fill porous uncompacted crystalline frameworks suggesting early, possibly syndepositional, precipitation (Figure S7). Despite the uncertain timing of formation, hanksite ages nonetheless provide the most internally consistent and reproducible ages in the Upper Salt. These ages are retained in the age model, as explained in more detail in section 6.1.4.

6.1.2 U-Th criteria for age selection

We applied two additional criteria aimed at identifying samples that were minimally affected by detrital contamination and thus most likely to have remained closed systems with respect to U and Th, following the approach of Chen et al. (2020).

First, we identified low-detritus samples by removing all samples with $^{230}Th/^{232}Th$ atomic ratios less than 36×10^{-6}. As the initial $^{230}Th/^{232}Th$ ratio is estimated to be $9 \pm 4 \times 10^{-6}$ in the Searles Basin (Lin et al., 1998), our criterion is equivalent to four times the estimated initial value. While the precise value of this criterion is subjective, it is intended to identify samples that are the most sensitive to corrections for initial ^{230}Th, producing imprecise age estimates and raising questions about the accuracy of corrected ages. In total, 18 samples were removed due to this criterion, including 16 that passed mineralogical selection criteria.

To identify samples that were most likely to have remained closed systems with respect to U and Th, we defined a final criterion using the initial $\delta^{234}U$ value calculated for the authigenic portion of each sample. $\delta^{234}U$ is expressed in units of per mil (‰) and is defined as

$$\delta^{234}U = (((^{234}U/^{238}U)-1)*1000 \quad (1)$$

where $(^{234}U/^{238}U)$ is an activity ratio. A sample at secular equilibrium has $(^{234}U/^{238}U)$ of 1 and a $\delta^{234}U$ of 0. "Initial" $\delta^{234}U$, or $\delta^{234}U_0$, is the $\delta^{234}U$ corrected for decay of ^{234}U since the formation of the mineral:

$$\delta^{234}U_0 = \delta^{234}U * e^{\lambda 234 * t} \quad (2)$$

where λ_{234} is the decay constant for ^{234}U (Cheng et al., 2013), and t is the age determined for the mineral from its U-Th data.

We then corrected $\delta^{234}U_0$ values for detrital U. We identified the fraction of detrital U using the measured $^{238}U/^{232}Th$ ratios and a detrital $^{238}U/^{232}Th$ ratio of 0.25 ± 0.10 (the ratio corresponding to a detrital $^{230}Th/^{232}Th$ ratio of $9\pm4 \times 10^{-6}$ and detrital matter with ^{230}Th and ^{238}U in secular equilibrium) (Chen et al., 2020). We assumed a $\delta^{234}U$ value of 0 for detrital U, and determined the initial $\delta^{234}U$ values necessary for non-detrital (authigenic) U to produce the initial $\delta^{234}U$ values determined for the bulk sample. We refer to these estimates of the initial $\delta^{234}U$ values of authigenic precipitates as $\delta^{234}U_{0,auth}$.

Unusually high values for $\delta^{234}U_{0,auth}$ indicate samples with anomalously old ages due to U loss, as the age correction will "overcorrect" measured $\delta^{234}U$ values for age decay. In order to use this criterion, however, we must first determine a reasonable range for $\delta^{234}U_{0,auth}$ values in Searles Basin precipitates.

Most natural waters have positive $\delta^{234}U$ values due to preferential leaching of ^{234}U from radiation-damaged sites and mineral surfaces (Chabaux et al., 2003). $\delta^{234}U$ values in rivers and closed-basin lakes vary due to changes in chemical and physical weathering intensity and/or changes in U source (Grzymko et al., 2007; McGee, 2012; Robinson et al., 2004). In the Searles Basin, $\delta^{234}U_{0,auth}$ values appear to have varied within a narrow range over the last 30 ka despite dramatic changes in temperature and precipitation accompanying the last glacial termination. $\delta^{234}U_{0,auth}$ values of samples that met the sedimentological criteria from the Lower Salt, Parting Mud and Upper Salt range from 191‰ to 281‰. We applied this range for the remainder of SLAPP-SRLS17 sediments. We excluded samples with $\delta^{234}U_{0,auth} > 290$‰, as these samples are

likely to have lost uranium, producing anomalously old ages. We identified 5 samples with $\delta^{234}U_{0,auth}$ values greater than 290‰, which includes 3 samples that passed all other criteria.

6.1.3 Evaluation of retained ages

Forty-six (46) ages were retained based on the sedimentological and U-Th criteria described above. The ages consisted primarily of halite in the Upper Salt and Lower Salt, aragonite in the Parting Mud, and gaylussite in the Bottom Mud and Mixed Layer (Figure S2). Ages from these samples are stratigraphically consistent, with limited exceptions discussed below (Figure 3B). The resulting age-depth dataset is also broadly consistent with previous dating of Searles Basin sediments, but with substantially reduced uncertainties (see Section 6.2.3) (Figure S1).

Importantly, gaylussite ages in the uppermost Bottom Mud (35-43 m) are consistent with nearby ages from primary salts (aragonite, halite), suggesting that gaylussite formed syndepositionally (within the precision of the age model) (Figure 3A, D). This observation lends confidence to our reliance on ages from gaylussite in the lowermost 30 m of the core.

We focus here on two remaining problems with dating samples. First, there is a wide range of ages in the Upper Salt, discussed in Section 6.1.4. Second, no ages were obtained between 51.03 m and 61.79 m due to a lack of samples that passed mineralogical and U-Th criteria. In Section 6.2.1, we refine the age model in this interval, which contains Termination II.

6.1.4 Upper Salt ages and the impact of solution mining

The ages of halite crystals in the Upper Salt included scatter beyond calculated measurement uncertainties (Figure 3). For example, at 18.08 m, ages range from 15.8 ± 0.5 to 20.1 ± 0.8 ka (n=3), and at 20.96 m ages range from 6.8 ± 0.7 to 18 ± 2 ka (n=3). We hypothesize that this lack of reproducibility reflects past mining operations in the Upper Salt. Mining operations prior

to the 1970s involved extracting brine from Searles Basin salt units. During the 1970s, extraction methods changed, and hot processed brines were reinjected into the Upper Salt to encourage salt dissolution and generate higher mineral yields. Brine was injected into the base of the Lower and Upper Salts under the assumption that the hot brine would rise through the salt. Brine flow therefore may have produced dissolution and reprecipitation of evaporite minerals, and in particular halite, the most soluble salt in Searles Basin deposits.

Partial dissolution of halite is likely to remove uranium and leave behind thorium, a process that would produce dates older than the true depositional age. Secondary precipitation of salts along crystal boundaries and in voids and fractures may also impact Upper Salt deposits; if included in dated samples, these secondary precipitates would bias dates to be younger than their depositional age. Even with removal of the outer surface of each sample during sample preparation, it is likely that Upper Salt halite samples incorporated secondary materials due to fractures and voids within crystals. As we cannot determine *a priori* which dates from Upper Salt halite samples are accurate, we reject all Upper Salt halite ages from the age model. We speculate that the divergence of ages observed here is also the reason that only one U-Th age has previously been reported from the Upper Salt (Peng et al., 1978).

To provide age constraints for the Upper Salt, we used hanksite ages. Hanksite forms large euhedral crystals less susceptible to dissolution and reprecipitation than smaller, more soluble halite and trona crystals with larger surface areas. Two hanksite samples from the same stratigraphic interval at 20.83 m gave similar ages (13.2 ± 0.2 and 14.1 ± 0.17 ka). While these ages do not agree within uncertainty, this difference plausibly reflects the duration of hanksite formation during diagenesis. These ages, therefore, should be considered minimum ages, which suggests that the transition from the Parting Mud to the Upper Salt occurred before 14.1 ka.

Assuming that high lake levels existed during mud deposition and that salt deposits reflect lower lake levels, Searles Lake level fell and disconnected from Owens and China Lake before 14.1 ka.

Shoreline data from China Lake support this conclusion. Rosenthal et al. (2017) demonstrated that China Lake and Searles Lake were interconnected between 17-14 ka. Radiocarbon dating of gastropod and mollusk shells in the China Lake Basin and uppermost Searles Basin (Salt Wells Valley) suggest diminished connection and declining lake levels in the Searles basin beginning at 14.1 ka. This age agrees with the oldest hanksite age from the Upper Salt and suggests that hanksite precipitation occurred shortly after the onset of lake level drawdown and Upper Salt deposition. While there may have been a brief rise of China Lake at ~13.2 ka, by 13-12.6 ka gastropods that inhabited spring discharge aprons indicate falling lake levels and exposure of groundwater seeps in the China Basin (Rosenthal et al., 2017).

We noted above that solution mining also took place in the Lower Salt, raising the question of why it did not produce similar effects on evaporite minerals in this unit. We hypothesize that mining had relatively less effect on Lower Salt ages due to the interlayered muds (Figure 1) that limited fluid flow between salt units.

6.2 Age model

Combining the various rejection criteria and mining history, we retained 37 U-Th ages to establish a chronology for the SLAPP-SLRS17 core. We constructed an age model with the Bayesian age-depth modeling program Bacon (Blaauw and Christen, 2011; Supplementary Material; Figure S8). We evaluated age-depth relationships using stratigraphic information and a proxy comparison.

6.2.1 Age model refinement and tie point establishment

We note two gaps in the age model (44.55 - 49.98 m and 51.03 - 61.79 m) that result in a lack of robust age constraints between 55-100 ka and 110-145 ka (Figure 3B and S9). The lower gap contains Termination II, the penultimate glacial termination. Previous work and our dating of SLAPP-SRLS17 demonstrates that Termination I (the most recent glacial termination) was accompanied by marked changes in lake level and sedimentation rates in Searles Basin (Lin et al., 1998; Phillips et al., 1994; Smith, 1979). Given evidence from southeastern California sites for basin desiccation and lowering of groundwater tables across both Termination I and II (Lowenstein et al., 1999; Wendt et al., 2018), there is reason to suspect that Termination II was also marked by changes in lake level and sedimentation rate in Searles Basin. However, without radiometric ages, the U-Th-based age model projects a linear sedimentation rate throughout the 110-145 ka interval (Figure 3).

Plant wax hydrogen isotope (δD_{wax}) measurements from SLAPP-SRLS17 sediments provide a means of refining the age model across Termination II. δD_{wax} values primarily track changes in precipitation δD values (Feakins and Sessions, 2010; Sachse et al., 2012). Similarly, regional speleothem $\delta^{18}O$ values are thought to primarily reflect changes in precipitation $\delta^{18}O$ values (Lachniet et al., 2014; Moseley et al., 2016). Assuming minimal lag in the record of precipitation $\delta^{18}O$ and δD recorded by speleothems and sedimentary plant waxes respectively, we expect good agreement between δD_{wax} and speleothem $\delta^{18}O$. During the last 100 ka, there is generally good correspondence (within age model uncertainty) between SLAPP-SLRS17 δD_{wax} and $\delta^{18}O$ changes recorded in the Devils Hole and Leviathan records (Lachniet et al., 2014; Moseley et al., 2016), with more positive values during warm periods (MIS5, MIS3, and MIS1)

and more negative values during the MIS4 and MIS2 glacial periods, as well as during MIS5d and MIS5b (Figure 4).

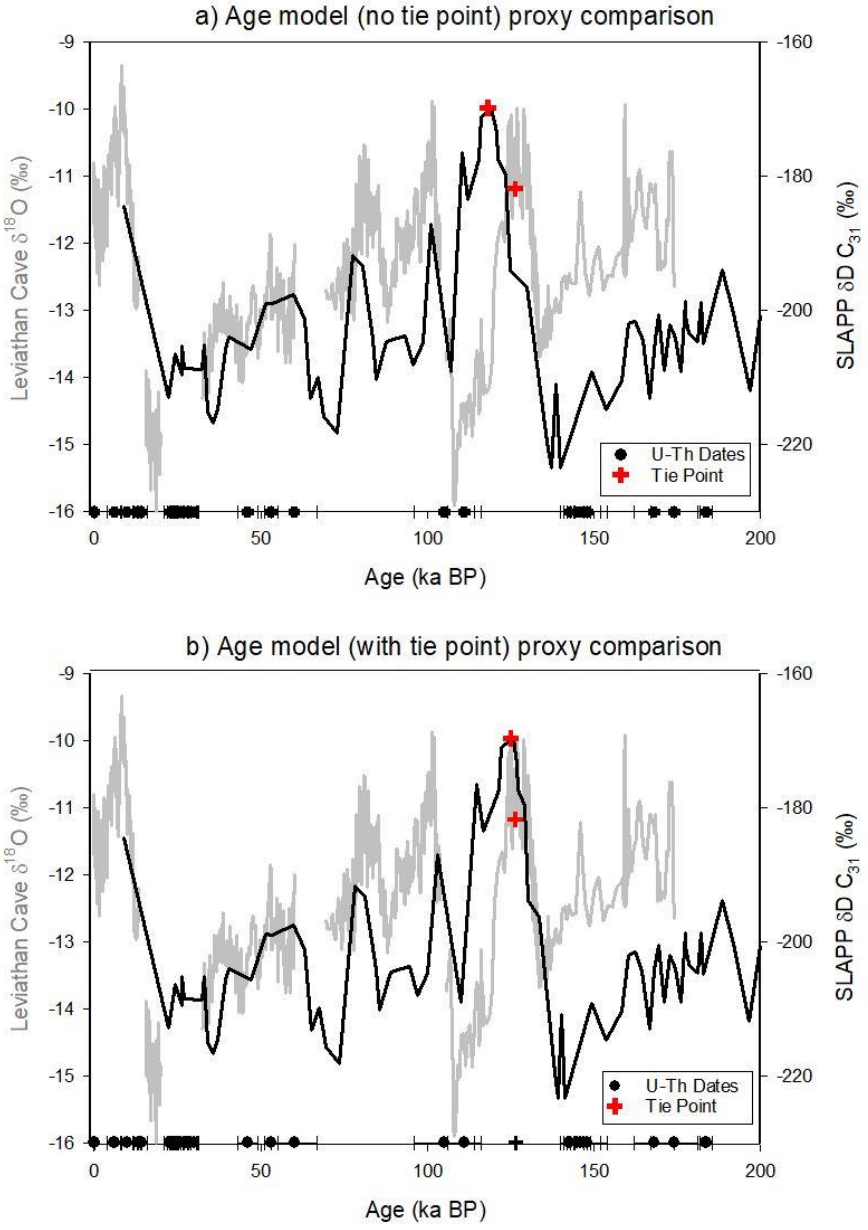

Figure 4. Evaluation of age model performance using comparison of SLAPP-SLRS17 C_{31} δD_{wax} (Peaple et al., 2022) and the Leviathan $\delta^{18}O$ compilation from Leviathan, Lehman and Pinnacle Caves (Lachniet, 2016). a)

There is good agreement over the last 100 ka, but an offset of ~10 ka exists at Termination II. This likely results from changing sedimentation rates which are unconstrained by a lack of U-Th ages between 110 and 145 ka in the SLAPP-SLRS17 record. We establish a tie point between the records (red cross) and apply it to produce a final age model (Figure 5). b) Comparison of Leviathan $\delta^{18}O$ and SLAPP-SLRS17 C_{31} δD_{wax} data using the age model with the tie point. Note that because Bacon does not force the age model to pass directly through the tie point, the median age of the tie point in the SLAPP-SRLS17 record is slightly offset from the median age of the tie point in the Leviathan record.

In contrast, we observe a clear discrepancy between SLAPP-SLRS17 δD_{wax} and regional speleothem $\delta^{18}O$ records during Termination II (Figure 4). While speleothem records show a steep rise in $\delta^{18}O$ values during Termination II and high values during MIS5e (Figure 4), an increase in SLAPP-SLRS17 δD_{wax} appears approximately 10 ka later on the U-Th age model. Based on the agreement in regional $\delta^{18}O$ records and the SLAPP-SLRS17 δD_{wax} record over the last 100 ka, we argue that this mismatch during Termination II reflects imprecision in the SLAPP-SLRS17 age model due to the lack of age constraints around this time. To address this gap, we introduce a tie point between the Leviathan speleothem $\delta^{18}O$ record (Lachniet et al., 2014) and the SLAPP-SRLS17 record at the peak of MIS5. We choose the Leviathan record because it is based on speleothems with minimal water transit times, whereas the Devils Hole calcite, precipitated from groundwater far from its primary recharge site, may lag due to longer transit times.

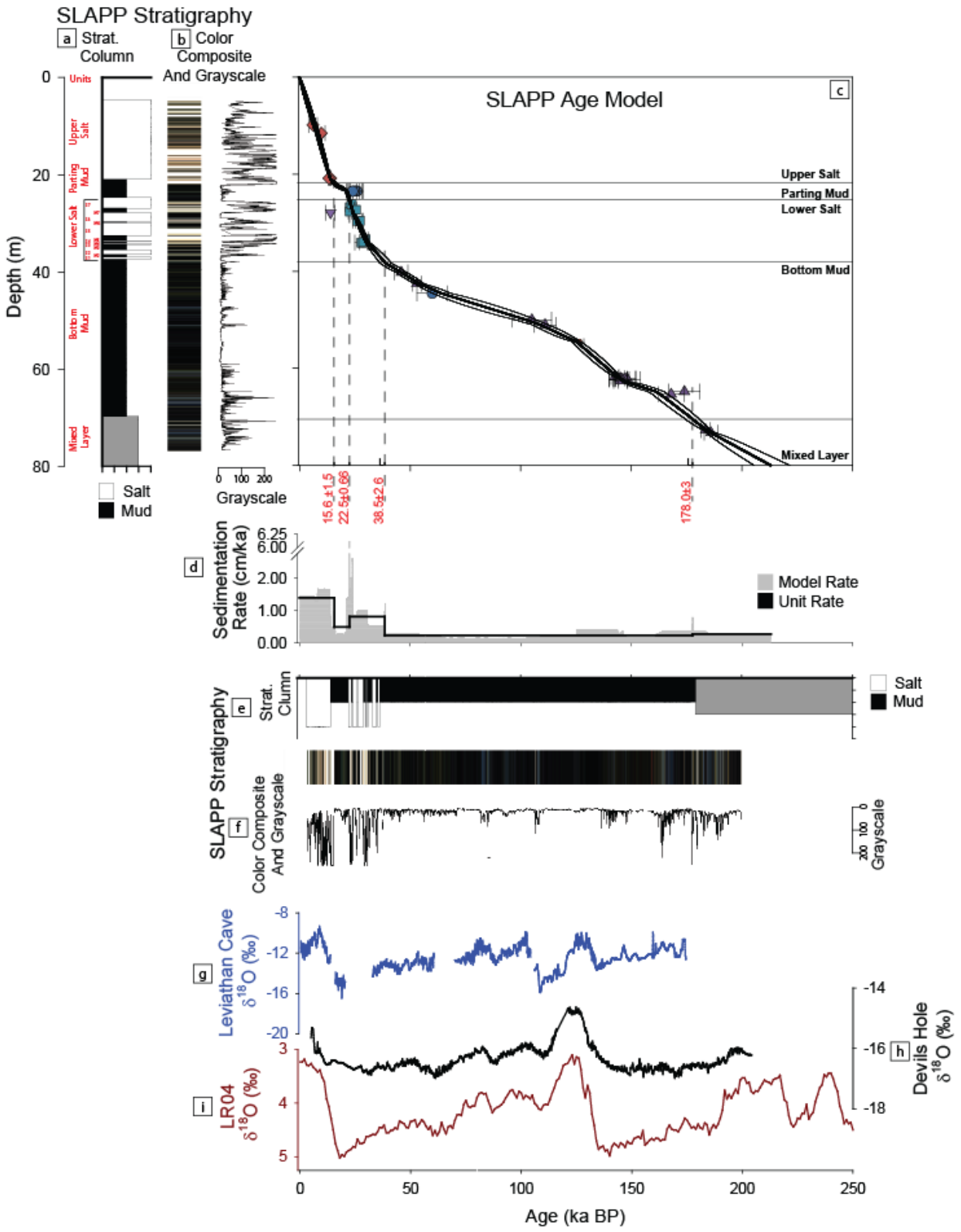
SLAPP Stratigraphy
a Strat. Column
b Color Composite And Grayscale
Depth (m)
Units
Upper Salt
Parting Mud
Lower Salt
Bottom Mud
Mixed Layer
Salt
Mud
Grayscale
SLAPP Age Model
c
Upper Salt
Parting Mud
Lower Salt
Bottom Mud
Mixed Layer
15.6±1.5
22.5±0.66
38.5±2.6
178.0±3
d
Sedimentation Rate (cm/ka)
Model Rate
Unit Rate
SLAPP Stratigraphy
e Strat. Clumn
Salt
Mud
f Color Composite And Grayscale
Grayscale
g Leviathan Cave δ18O (‰)
h Devils Hole δ18O (‰)
i LR04 δ18O (‰)
Age (ka BP)

618

Figure 5. Age-depth relationship for the SLAPP-SLRS17 core. a) General stratigraphy; b) core color composite and grayscale profile; c) final age model, using 37 U-Th ages and the tie point, constructed with Bacon using optimized model parameters (See main text and Supplementary Material). Model mean and 95% confidence interval shown. Changes in model slope correspond to different units and changes in sedimentation rate. d) Sedimentation rate extracted from the age model (gray) and sedimentation rate by unit (black). e and f) SLAPP-SLRS17 stratigraphy and grayscale data plotted with g) Leviathan, h) Devils Hole, and i) LR04 stack records (Lachniet, 2016; Lisiecki and Raymo, 2005; Moseley et al., 2016).

We established a tie point near Termination II by matching the peak nearest to 125 ka in the SLAPP-SRLS17 plant wax C_{31} alkane δD record to the MIS5e peak in the Leviathan speleothem $\delta^{18}O$ compilation (Figure 4 and Supplementary Material). We scaled and interpolated the data before applying a low pass filter to both records to remove high frequency variability and then calculated the second derivatives to identify a match point at a gradient of 0. The tie point indicates an age of 126.5 ka at 54.5 m depth for the SLAPP-SLRS17 record. We assign an error of 2 ka to this tie point. Age uncertainties in the Leviathan record are mostly between 0.2 and 0.5 ka (2σ), and the largest uncertainties are ~0.9 ka (Lachniet, 2016). Our assigned error is intended to account for uncertainties in the Leviathan record and the correlation between records. Furthermore, the magnitude of the assigned error is consistent with the errors of other ages in the SLAPP-SLRS17 record. The SLAPP-SLS17 C_{31} δD_{wax} record has a resolution of 2.8 ka^{-1}. Since there are approximately 25 ka between the start of Termination II and the end of the last interglacial, the SLAPP-SLRS17 C_{31} δD_{wax} record has ample resolution to accurately determine the stationary point of the interglacial. We incorporated the tie point age, error, and depth into the Bacon age model (Figure 5).

The introduction of a tie point results in substantially higher sedimentation rates during the end of MIS6 and a reduction in sedimentation rates during the first half of MIS5. The introduction of the tie point has minimal impacts on the primary scientific goals of the SLAPP-SRLS17 record; its primary impact is to remove leads and lags between the Searles Basin and other regional records during Termination II.

6.2.2 Sedimentation rates

In the Searles Basin, evaporite deposition rates outpaced those of muds. Rapid deposition of salt is observed in modern basins such as the Dead Sea where 2 m of halite was deposited within ~40 years as water levels fell ~30 m since 1980 (Lensky et al., 2005; Lowenstein et al., 2021). In Death Valley, California, a 186 m-long core from the center of Badwater Basin had an average sedimentation rate of 1 m/ka. Evaporite minerals (predominantly halite) were deposited much faster (~1.7-3.8 m/ka) and mud deposition was slower (0.4-1 m/ka) (Lowenstein et al., 1999). In the SLAPP-SLRS17 record, average accumulation rates for the units vary accordingly (Figure 5): Upper Salt (~1.4 m/ka), Parting Mud (0.5 m/ka), Lower Salt (0.8 m/ka), Bottom Mud (0.2 m/ka), Mixed Layer (0.4 m/ka).

We note several limitations in our characterization of sedimentation rates. While the age model indicates a higher sedimentation rate in the Lower Salt compared to the Bottom Mud, the core has many changes in lithology (Figure 1) which may correspond to sedimentation rate changes. The Lower Salt, for example, contains seven alternating salts (S1-S7) and muds (M2-M7) (Figure 1). These subunits range in thickness from ~18 cm to 220 cm. Cumulatively, the unit contains approximately 650 cm of salt and 420 cm of mud. Despite our best efforts to isolate minerals, viable samples are generally spaced more widely than the units and are not necessarily located near subunit boundaries. Thus, the sedimentation rate suggested by the age model is

represented as an average rate across lithologies, providing a maximum rate of mud deposition and a minimum rate of evaporite deposition.

6.2.3 Comparison with previous Searles Basin chronologies

The SLAPP-SRLS17 age model reproduces the broad features of prior dating of Searles Basin sediments (Supplementary Material Section 1). The Upper Salt broadly spans from late deglaciation to the late Holocene; the Parting Mud was deposited during the Last Glacial Maximum and early deglaciation; the Lower Salt spans the latter part of MIS3 through the Last Glacial Maximum; and the Bottom Mud extends back through the last interglacial (MIS5) and beyond. However, closer comparison shows many significant differences in age and analytical uncertainty. Individual U-Th ages from this study have substantially lower uncertainties than ages from previous work, due to improvements in U-Th geochronology—chiefly the switch from alpha decay counting to measurement by inductively coupled plasma mass spectrometry. Through the careful application of sedimentological and U-Th criteria, we are also able to identify the dates that most closely reflect depositional ages, reducing scatter in the age-depth relationship.

In the Upper Salt, near the Upper Salt-Parting Mud boundary, an age from Peng et al. (1978) is ~5-6 ka younger than those from the SLAPP-SRLS17 record, perhaps due to inclusion of secondary salts in the large (>10 g) Peng et al. sample. An additional key new finding is that Termination II occurs in the Bottom Mud rather than at the Bottom Mud/Mixed Layer contact as suggested by Bischoff et al. (1985). The new age model suggests that the Bottom Mud/Mixed Layer contact instead occurs at 178 ± 3 ka, agreeing within uncertainty with the timing of lake level rise in the Death Valley basin at the beginning of MIS6 (186 ± 17 ka; Lowenstein et al., 1999). Related to this finding, we observe that many of the gaylussite ages from Bischoff et al.

(1985) are systematically younger than samples from similar depths in SLAPP-SRLS17. While some of this difference may reflect differences in sedimentation rates between the two core sites, the samples from Bischoff et al. (1985) included secondary salts with much younger ages, such as the nahcolite from near the Bottom Mud-Mixed Layer boundary, also dated in this study (Figure 3A).

6.3 Lessons for future work using U-Th on lake precipitates

This study shows that U-Th dating of lacustrine evaporites must take into account mineralogical and textural information. U-Th dates from minerals that form during or very soon after deposition provide useful constraints on sediment ages, whereas later precipitating minerals only provide minimum ages. In addition, mineral textures and stratigraphic associations (e.g., crystal distribution controlled by surrounding sedimentary layers versus crystals that crosscut these layers) provide essential information as to the reliability of associated U-Th ages. In the present study, dating and mineralogical observations were conducted concurrently; it would have been more efficient to conduct mineralogical observations first, and to focus U-Th dating on minerals more likely to have behaved as closed systems and to provide syndepositional ages.

U-Th ages of many different mineralogies and textures can provide information beyond chronology for the sedimentary record. They can be applied to demonstrate secondary crystal formation and even distinguish between primary and secondary textures. For example, our sedimentological criteria excluded trona from our age model, but ages from trona samples are in close agreement with the model, suggesting that they were formed concurrently with deposition (Figure 3A). Thus, we can conclude the textures are primary.

Second, we suggest various quality control tests for identifying the most reliable U-Th ages, applying a similar approach to Chen et al. (2020). Here, we use the $^{230}Th/^{232}Th$ ratio to identify samples with low detrital contamination, and we use the initial $\delta^{234}U$ value of authigenic material along with reproducibility to identify samples that have been likely to have remained closed systems with respect to U and Th.

Third, we note the utility of screening for ^{238}U and ^{232}Th concentrations in all samples prior to U-Th dating. This screening was essential for identifying samples with low detrital content and for determining appropriate sample and spike amounts for dating, given the very wide range of ^{238}U and ^{232}Th concentrations in our samples due to varying mineralogy and lake conditions. The time added by screening is a small fraction of the time spent conducting full U-Th sample preparation and analysis on samples with low $^{238}U/^{232}Th$ ratios or samples with over- or underestimated ^{238}U contents.

Finally, we argue that tie points may still be necessary in U-Th-based age models for lake sediments (e.g., Rodbell et al., 2022), but that these should be introduced as sparingly as possible, and with thoughtful consideration as to what scientific questions are removed from consideration once the age model has been tuned to other time series.

7 Conclusion

The diverse evaporite mineralogy of the Searles Basin enables insights into past lake conditions, but poses significant challenges in establishing a robust chronology because of an array of deposition and diagenetic sequences. Thus, extensive evaluation and clear criteria must be applied to determine ages appropriate for dating the sediments. Our U-Th dating of 98 samples

covering 9 different mineral categories validates interpretations that some groups are primary or syndepositional, while other minerals are secondary (ages younger than depositional ages) or subject to post-depositional U loss (ages older than depositional ages). Our criteria target syndepositional materials with low detrital contamination, uranium isotope data consistent with closed-system behavior, and good reproducibility in a given depth range. We used 37 ages for age model construction using the Bayesian age-depth modeling package Bacon with carefully chosen parameters that account for stratigraphic changes in the core.

We find that the SLAPP-SRLS17 record extends to >200 ka, recording 2 full glacial interglacial cycles. We chose to include a tie point during Termination II between plant wax δD data from the core to the Leviathan speleothem $\delta^{18}O$ record to fill an important chronological gap in the record where no datable material was available. This single tie point reduces the ability to use the record for studies of the precise phasing of events across Termination II but preserves the ability to study orbital signals and glacial-interglacial variability in the dataset. The age model lays the foundation for further work using Searles Basin sediments to probe the hydrological and ecological history of the region, and provides several lessons learned for future work using U-Th dating to develop high-quality chronologies from evaporite minerals.

Acknowledgements

This study was supported by U.S. National Science Foundation Grant NSF-EAR – 1903519, 1903544, 1903659 and 1903665 respectively to Stroup, McGee, Lowenstein and Feakins and a Comer Science and Education Foundation Grant to McGee and Lowenstein. We thank Searles Valley Minerals and especially Jade Zimmerman for access, logistical support and local knowledge of the site. We thank Joe Jannick for assistance during on-site drilling and during

initial core description. Support was provided by the Continental Scientific Drilling (CSD) Facility, University of Minnesota, during core collection and during the initial core description, especially Ryan O'Grady, Kristina Brady, Mark Shapley, and Anders Noren. Special thanks to Maarten Blaauw for consultations regarding Bacon and its application to this sedimentary environment.

Author contribution statement: JS, DM, SF, and TL acquired funding; JS, DM, KO, and CYC assisted with on-site drilling of the SLAPP-SRLS17 core; JS, DM, AJ, CYC and HM conducted core sampling, U-Th sample preparation, analyses and/or data interpretation; KO and TL developed the mineralogical and stratigraphic interpretations; SF and MP conducted the biomarker analyses; JS, DM and KO developed the first draft of the manuscript; all authors contributed to the text and interpretations.

Conflict of Interest

The authors declare no financial conflicts of interests for any author or their affiliations.

Open Research

Data files are archived at the NOAA paleoclimatology database (Stroup et al., 2022).

References

Bacon, S. N., Burke, R. M., Pezzopane, S. K., and Jayko, A. S., 2006, Last glacial maximum and Holocene lake levels of Owens Lake, eastern California, USA: Quaternary Science Reviews, v. 25, no. 11-12, p. 1264-1282.

776 Bacon, S. N., Jayko, A. S., Owen, L. A., Lindvall, S. C., Rhodes, E. J., Schumer, R. A., and
777 Decker, D. L., 2020, A 50,000-year record of lake-level variations and overflow from
778 Owens Lake, eastern California, USA: Quaternary Science Reviews, v. 238, p. 106312.
779 Bader, N. E., 2000, Pollen analysis of Death Valley sediments deposited between 166 and 114
780 ka: Palynology, v. 24, no. 1, p. 49-61.
781 Benson, L. V., Currey, D. R., Dorn, R. I., Lajoie, K. R., Oviatt, C. G., Robinson, S. W., Smith, G.
782 I., and Stine, S., 1990, Chronology of expansion and contraction of four Great Basin lake
783 systems during the past 35,000 years: Palaeogeography, Palaeoclimatology,
784 Palaeoecology, v. 78, no. 3-4, p. 241-286.
785 Bischoff, J. L., Rosenbauer, R. J., and Smith, G. I., 1985, Uranium-series dating of sediments
786 from Searles Lake: differences between continental and marine climate records:
787 Science, v. 227, no. 4691, p. 1222-1224.
788 Blaauw, M., and Christen, J. A., 2011, Flexible paleoclimate age-depth models using an
789 autoregressive gamma process: Bayesian Analysis, v. 6, no. 3, p. 457-474.
790 Chabaux, F., Riotte, J., and Dequincey, O., 2003, U-Th-Ra fractionation during weathering and
791 river transport: Reviews in Mineralogy and geochemistry, v. 52, no. 1, p. 533-576.
792 Chen, C. Y., McGee, D., Woods, A., Pérez, L., Hatfield, R. G., Edwards, R. L., Cheng, H.,
793 Valero-Garcés, B. L., Lehmann, S. B., and Stoner, J. S., 2020, U-Th dating of lake
794 sediments: Lessons from the 700 ka sediment record of Lake Junín, Peru: Quaternary
795 Science Reviews, v. 244, p. 106422.
796 Cheng, H., Edwards, R. L., Shen, C.-C., Polyak, V. J., Asmerom, Y., Woodhead, J., Hellstrom,
797 J., Wang, Y., Kong, X., and Spötl, C., 2013, Improvements in 230Th dating, 230Th and
798 234U half-life values, and U–Th isotopic measurements by multi-collector inductively
799 coupled plasma mass spectrometry: Earth and Planetary Science Letters, v. 371, p. 82-
800 91.
801 Feakins, S. J., and Sessions, A. L., 2010, Controls on the D/H ratios of plant leaf waxes in an
802 arid ecosystem: Geochimica et Cosmochimica Acta, v. 74, no. 7, p. 2128-2141.
803 Grzymko, T. J., Marcantonio, F., McKee, B. A., and Stewart, C. M., 2007, Temporal variability of
804 uranium concentrations and 234U/238U activity ratios in the Mississippi river and its
805 tributaries: Chemical Geology, v. 243, no. 3-4, p. 344-356.
806 Hardie, L. A., Lowenstein, T. K., and Spencer, R. J., The problem of distinguishing between
807 primary and secondary features in evaporites, *in* Proceedings Sixth international
808 symposium on salt1985, Volume 1, Salt Institute Alexandria, VA, p. 11-39.
809 Heusser, L. E., Kirby, M. E., and Nichols, J. E., 2015, Pollen-based evidence of extreme drought
810 during the last Glacial (32.6–9.0 ka) in coastal southern California: Quaternary Science
811 Reviews, v. 126, p. 242-253.
812 Jaffey, A., Flynn, K., Glendenin, L., Bentley, W. t., and Essling, A., 1971, Precision
813 measurement of half-lives and specific activities of U 235 and U 238: Physical review C,
814 v. 4, no. 5, p. 1889.
815 Jannik, N. O., Phillips, F. M., Smith, G. I., and Elmore, D., 1991, A 36Cl chronology of lacustrine
816 sedimentation in the Pleistocene Owens River system: Geological Society of America
817 Bulletin, v. 103, no. 9, p. 1146-1159.
818 Knott, J. R., Liddicoat, J. C., Coe, R. S., and Negrini, R. M., 2019, Radiocarbon and
819 paleomagnetic chronology of the Searles Lake Formation, San Bernardino County,
820 California, USA, From Saline to Freshwater: the Diversity of Western Lakes in Space
821 and Time, Geological Society of America Special.
822 Ku, T.-L., Luo, S., Lowenstein, T. K., Li, J., and Spencer, R. J., 1998, U-series chronology of
823 lacustrine deposits in Death Valley, California: Quaternary Research, v. 50, no. 3, p.
824 261-275.

Lachniet, M., 2016, A Speleothem Record of Great Basin Paleoclimate: The Leviathan Chronology, Nevada, Developments in Earth Surface Processes, Volume 20, Elsevier, p. 551-569.
Lachniet, M. S., Denniston, R. F., Asmerom, Y., and Polyak, V. J., 2014, Orbital control of western North America atmospheric circulation and climate over two glacial cycles: Nature communications, v. 5, no. 1, p. 1-8.
Lensky, N., Dvorkin, Y., Lyakhovsky, V., Gertman, I., and Gavrieli, I., 2005, Water, salt, and energy balances of the Dead Sea: Water Resources Research, v. 41, no. 12.
Liddicoat, J. C., Opdyke, N. D., and Smith, G. I., 1980, Palaeomagnetic polarity in a 930-m core from Searles Valley, California.
Lin, J. C., Broecker, W. S., Hemming, S. R., Hajdas, I., Anderson, R. F., Smith, G. I., Kelley, M., and Bonani, G., 1998, A reassessment of U-Th and 14 C ages for late-glacial high-frequency hydrological events at Searles Lake, California: Quaternary Research, v. 49, no. 1, p. 11-23.
Lisiecki, L. E., and Raymo, M. E., 2005, A Pliocene-Pleistocene stack of 57 globally distributed benthic δ18O records: Paleoceanography, v. 20, no. 1.
Litwin, R. J., Smoot, J. P., Durika, N. J., and Smith, G. I., 1999, Calibrating Late Quaternary terrestrial climate signals: radiometrically dated pollen evidence from the southern Sierra Nevada, USA: Quaternary Science Reviews, v. 18, no. 10-11, p. 1151-1171.
Lora, J. M., Mitchell, J. L., Risi, C., and Tripati, A. E., 2017, North Pacific atmospheric rivers and their influence on western North America at the Last Glacial Maximum: Geophysical Research Letters, v. 44, no. 2, p. 1051-1059.
Lowenstein, T. K., and Hardie, L. A., 1985, Criteria for the recognition of salt-pan evaporites: Sedimentology, v. 32, no. 5, p. 627-644.
Lowenstein, T. K., Li, J., Brown, C., Roberts, S. M., Ku, T.-L., Luo, S., and Yang, W., 1999, 200 ky paleoclimate record from Death Valley salt core: Geology, v. 27, no. 1, p. 3-6.
Lowenstein, T. K., Weldeghebriel, M. F., Sirota, I., Eyal, H., Mor, Z., and Lensky, N. G., 2021, Criteria for the recognition of clastic halite: The modern Dead Sea shoreline: Sedimentology, v. 68, no. 6, p. 2253-2269.
McGee, D., 2012, Absolute-dated, high-resolution records of water balance changes during the last glacial period and deglaciation from lacustrine cave deposits in the Bonneville Basin, Utah, USA: Quaternary International, v. 279, p. 317.
McGee, D., Moreno-Chamarro, E., Marshall, J., and Galbraith, E., 2018, Western US lake expansions during Heinrich stadials linked to Pacific Hadley circulation: Science advances, v. 4, no. 11, p. eaav0118.
Moseley, G. E., Edwards, R. L., Wendt, K. A., Cheng, H., Dublyansky, Y., Lu, Y., Boch, R., and Spötl, C., 2016, Reconciliation of the Devils Hole climate record with orbital forcing: Science, v. 351, no. 6269, p. 165-168.
Munroe, J. S., and Laabs, B. J., 2013, Temporal correspondence between pluvial lake highstands in the southwestern US and Heinrich Event 1: Journal of Quaternary Science, v. 28, no. 1, p. 49-58.
Olson, K. J., and Lowenstein, T. K., 2021, Searles Lake evaporite sequences: Indicators of late Pleistocene/Holocene lake temperatures, brine evolution, and p CO2: Bulletin, v. 133, no. 11-12, p. 2319-2334.
Oster, J. L., Ibarra, D. E., Winnick, M. J., and Maher, K., 2015, Steering of westerly storms over western North America at the Last Glacial Maximum: Nature Geoscience, v. 8, no. 3, p. 201-205.
Oster, J. L., Montañez, I. P., Mertz-Kraus, R., Sharp, W. D., Stock, G. M., Spero, H. J., Tinsley, J., and Zachos, J. C., 2014, Millennial-scale variations in western Sierra Nevada precipitation during the last glacial cycle MIS 4/3 transition: Quaternary Research, v. 82, no. 1, p. 236-248.

Peaple, M. D., Bhattacharya, T., Lowenstein, T., McGee, D., Olson, K., Stroup, J. S., Tierney, J. E., and Feakins, S. J., 2022, Biomarker and pollen evidence for late Pleistocene pluvials in the Mojave Desert: Earth and Space Science Open Archive, p. 45.

Peng, T.-H., Goddard, J., and Broecker, W., 1978, A Direct Comparison of 14C and 230Th Ages at Searles Lake, California1: Quaternary Research, v. 9, no. 3, p. 319-329.

Phillips, F. M., Campbell, A. R., Smith, G. I., and Bischoff, J. L., 1994, Interstadial climatic cycles: A link between western North America and Greenland?: Geology, v. 22, no. 12, p. 1115-1118.

Phillips, F. M., Smith, G. I., Bentley, H. W., Elmore, D., and Gove, H. E., 1983, Chlorine-36 dating of saline sediments: preliminary results from Searles Lake, California: Science, v. 222, no. 4626, p. 925-927.

Prado-Pérez, A., Vázquez, M. C., Vargas, M. J., Sánchez, A. M., and del Villar, L. P., 2013, Sample quality index to preselect suitable carbonate samples for alpha spectrometry U/Th dating: Applied Radiation and Isotopes, v. 73, p. 32-43.

Reheis, M. C., Adams, K. D., Oviatt, C. G., and Bacon, S. N., 2014, Pluvial lakes in the Great Basin of the western United States—A view from the outcrop: Quaternary Science Reviews, v. 97, p. 33-57.

Reimer, P. J., Austin, W. E., Bard, E., Bayliss, A., Blackwell, P. G., Ramsey, C. B., Butzin, M., Cheng, H., Edwards, R. L., and Friedrich, M., 2020, The IntCal20 Northern Hemisphere radiocarbon age calibration curve (0–55 cal kBP): Radiocarbon, v. 62, no. 4, p. 725-757.

Robinson, L. F., Henderson, G. M., Hall, L., and Matthews, I., 2004, Climatic control of riverine and seawater uranium-isotope ratios: Science, v. 305, no. 5685, p. 851-854.

Rodbell, D., Hatfield, R., Abbott, M., Chen, C., Woods, A., Stoner, J., McGee, D., Tapia, P., Bush, M., and Valero-Garcés, B., 2022, 700,000 years of tropical Andean glaciation: Nature, p. 1-6.

Rosenthal, J. S., Meyer, J., Palacios-Fest, M. R., Young, D. C., Ugan, A., Byrd, B. F., Gobalet, K., and Giacomo, J., 2017, Paleohydrology of China Lake basin and the context of early human occupation in the northwestern Mojave Desert, USA: Quaternary Science Reviews, v. 167, p. 112-139.

Sachse, D., Billault, I., Bowen, G. K., Chikaraishi, Y., Dawson, T. E., Feakins, S. J., Freeman, K. H., Magill, C. R., McInerney, F. A., and Van Der Meer, M. T., 2012, Molecular paleohydrology: interpreting the hydrogen-isotopic composition of lipid biomarkers from photosynthesizing organisms: Annual Review of Earth and Planetary Sciences, v. 40, p. 221-249.

Smith, G. I., 1979, Subsurface stratigraphy and geochemistry of late Quaternary evaporites, Searles Lake, California, US Govt., 130 p.:

Smith, G. I., 1984, Paleohydrologic regimes in the southwestern Great Basin, 0–3.2 my ago, compared with other long records of “gobal” climate: Quaternary Research, v. 22, no. 1, p. 1-17.

Smith, G. I., 2009, Late Cenozoic geology and lacustrine history of Searles Valley, Inyo and San Bernardino Counties, California, US Geological Survey.

Smith, G. I., Barczak, V., Moulton, G. F., and Liddicoat, J. C., 1983, Core KM-3, a surface-to-bedrock record of late Cenozoic sedimentation in Searles Valley, California: USGPO, 2330-7102.

Stroup, J. S., Olson, K., Lowenstein, T. K., Adam, B. J., Mosher, H. M., Peaple, M., Feakins, S. J., Chen, C. Y., Lund, S. P., and McGee, D., 2022, https://www.ncdc.noaa.gov/paleo/study/xxxxx.

Tabor, C., Lofverstrom, M., Oster, J., Wortham, B., de Wet, C., Montañez, I., Rhoades, A., Zarzycki, C., He, C., and Liu, Z., 2021, A mechanistic understanding of oxygen isotopic changes in the Western United States at the Last Glacial Maximum: Quaternary Science Reviews, v. 274, p. 107255.

Thompson, R. S., and Anderson, K. H., 2000, Biomes of western North America at 18,000, 6000 and 0 14C yr BP reconstructed from pollen and packrat midden data: Journal of Biogeography, v. 27, no. 3, p. 555-584.
Trachsel, M., and Telford, R. J., 2017, All age–depth models are wrong, but are getting better: The Holocene, v. 27, no. 6, p. 860-869.
Wendt, K. A., Dublyansky, Y. V., Moseley, G. E., Edwards, R. L., Cheng, H., and Spotl, C., 2018, Moisture availability in the southwest United States over the last three glacial-interglacial cycles: Sci Adv, v. 4, no. 10, p. eaau1375.
Woolfenden, W. B., 2003, A 180,000-year pollen record from Owens Lake, CA: terrestrial vegetation change on orbital scales: Quaternary Research, v. 59, no. 3, p. 430-444.

Supplementary References

Christen, J. A., and Pérez, S., 2009, A new robust statistical model for radiocarbon data: Radiocarbon, v. 51, no. 3, p. 1047-1059.